Tension-compression asymmetry in plasticity of nanotwinned 3C-SiC nanocrystals

Saeed Zare Chavoshi[1*], Shuozhi Xu[2]

[1]Department of Mechanical Engineering, Imperial College London, London SW7 2AZ, UK

[2]California NanoSystems Institute, University of California, Santa Barbara, Santa Barbara, CA 93106-6105, USA

*Corresponding author: *s.zare@imperial.ac.uk*

Abstract

Encompassing nanoscale thin twins in metals induces diverse influences, either strengthening triggered by the lattice dislocation blockage effects or softening prompted by dislocation emission from coherent twin boundary (CTB)/grain boundary (GB) intersections as well as CTB migration; yet the deformation mechanism remains poorly understood in ceramic nanostructures possessing covalent bonds. Here, we report the results of uniaxial compressive and tensile stress loading of twin-free and nanotwinned nanocrystalline 3C-SiC ceramic attained by large-scale molecular dynamics simulations. We find a strong yet unique tension-compression asymmetry in strength of nanocrystalline ceramics, much higher than those of metals. We demystify that strength and ductility behaviour do not correlate simply with the amount of dislocation density, volume fraction of voids, volume fraction of intergranular disordered phase, and total strain energy; instead, it arises from a complex interplay of the aforementioned features and structural characteristics, e.g., GB and triple junction area distribution along/normal to the direction of straining as well as the capability of strain accommodation by the GBs and CTBs, with the dominant role of the structural characteristics in nanotwinned samples. Our results also reveal that primarily intergranular crack propagation and fracture along the GBs transpires in the samples, and not along the CTBs, resulting from

the high energy of the GBs. However, a high density of nanoscale twins in the 3C-SiC nanocrystals could give rise to the alternation of the crack path from intergranular to intragranular type induced by shear, which brings about the glide of Shockley partials along the CTBs and subsequent formation of CTB steps and twin plane migration.

I. Introduction

Ultrafine-grained (UFG) and nanocrystalline metals whose grains accommodate nanoscale thin twins divided by coherent twin boundaries (CTBs) have attracted much interest in the area of materials research owing to their high strength, good ductility, and high electrical conductivity, which is favourable for the applications in micro/nanoelectromechanical systems. In face-centered cubic (fcc) and diamond cubic lattices, a CTB is one of the $\sum 3$ coincidence-sitelattice boundaries with a <011> misorientation axis. As a high-angle grain boundary (GB), CTBs generate high barriers to dislocation gliding on inclined slip planes. Hence, CTBs can induce a 'Hall-Petch-like' effect leading to strengthening of nanotwinned materials. Nevertheless, there exists a critical CTB spacing λ, below which the strength of the nanotwinned material decreases with decreasing λ [1]. On the other hand, CTBs introduce strength softening effects in some metals, e.g., W [2-4], by providing nucleation sites for dislocations or migrating during the deformation process.

Tension-compression (T-C) asymmetry in plasticity and strength of nanocrystalline and UFG metals is of particular interest, which is indeed not evident in coarse grain metals [5]. This phenomenon has been extensively explored experimentally and computationally, yet the majority of prior studies of nanocrystalline materials focused on twin-free nanocrystalline samples. For instance, Cheng and colleagues [6] proposed a pressure dependent analytical model based on the bow-out of a GB dislocation source, demonstrating a gradual increase in

T-C asymmetry with decreasing grain size. The study carried out by Lund and co-workers [7, 8] established that Ni nanocrystals have higher strength in compression than in tension during uniaxial and biaxial deformation. Tang *et al.* [9] identified the brittle intergranular failure and GB separation in nanocrystalline tantalum during tensile loading whereas considerable plastic deformation within the grains was observed during compressive loading. Tomar and Zhou [10] showed that the yield strength asymmetry in nanocrystalline α-Fe_2O_3-fcc Al composites is related to the differences in GB sliding behaviour. Tschopp *et al.* [11] elaborated on the role of GB structure and reported that the average nucleation stress of Cu for all $< 110 >$ symmetric tilt GBs is over three times higher in compression than in tension over a range of strain rates. Nevertheless, Zhang and co-investigators [5] found that the Cu bicrystal samples with non-planar structured GBs have a higher tensile strength than the compressive one.

Despite a number of studies on T-C asymmetry in plasticity and strength of nanocrystalline materials, less progress about the nanotwinned nanocrystals has been achieved. A few recent work has addressed the influence of twin boundaries in T-C asymmetry of nanocrystals. Tucker *et al.* [12] examined the uniaxial deformation behaviour of $< 100 >$ columnar nanocrystalline Cu and discovered that in Cu nanocrystals containing high density of nanoscale twins, twin boundary migration is a dominant mode of plasticity, particularly during compressive deformation. Furthermore, Zhang and Zhou [13] discovered that the flow stresses of nanocrystalline Ni nanowire with different λ are higher under compression than under tension, with a minimum asymmetry at a particular λ, arising from the interplay of various dislocations mechanisms. Notwithstanding these studies, there exist open key questions in the area of nanotwinned nanocrystals, including how and how much the CTBs affect the T-C asymmetry in plasticity and strength of different nanocrystalline materials, particularly nanocrystalline ceramics where dislocation activities are less pronounced compared with metals owing to their strong covalent or ionic bonding [14]. Indeed, there is scarcity of research on the nanotwinned

ceramic materials subjected to various forms of loadings. Silicon carbide (SiC) is a well-known high strength ceramic with potential applications to extreme conditions of pressure, temperature, and wear such as nuclear energy systems, gas turbines, and special microelectronics due to its excellent properties of high radiation tolerance, high strength, high thermal conductivity, high chemical stability, high resistance to shock, low thermal expansion, low density, high refractive index and chemical inertness [15-19]. Accordingly, SiC is believed to be a potential replacement to leading horse material Si [20-23] on many applications. In particular, the cubic silicon carbide (3C-SiC), as a zinc blende structured SiC, possesses the highest fracture toughness, hardness, electron mobility, and electron saturation velocity amongst all SiC polytypes [17]. In spite of its importance, no experimental/computational observations have been reported in the literature to date documenting the T-C asymmetry behaviour of 3C-SiC nanocrystals comprising nanosized twins. There is therefore a need to conduct research both on experimental and theoretical grounds to provide valuable insights into the uniaxial deformation behaviour of such nanostructured ceramics. Motivated by this, in the current work, we carry out molecular dynamics (MD) simulation to characterize the atomic-level origins of T-C asymmetry and interactions amongst plasticity mechanisms in twin-free 3C-SiC nanocrystals as well as those containing nanoscale {111} twins.

II. Simulation methodology

MD simulations are implemented using the open source LAMMPS code [24]. As the validity of MD simulations considerably hinges on the choice of interatomic potential, it is crucial to employ an appropriate interatomic potential so as to attain accurate results [25-30]. Atomic interactions of SiC are modelled using the effective many-body interatomic potential developed by Vashishta *et al.* [31], which is capable of reasonably reproducing the generalized stacking fault energies, cohesive energy, elastic constants, and melting point of 3C-SiC. The initial

nanocrystalline structure is generated using a Voronoi tessellated method [32]. An example of the periodic 3D nanotwinned nanocrystalline 3C-SiC structure is illustrated in Figure 1(a), where atoms are coloured according to a structure identification algorithm for diamond lattice [33]. The $\sum 3$ CTBs in nanotwinned 3C-SiC lie on {111} planes, similar to those in an fcc lattice. A schematic illustration of the atomic arrangement of {111} $\sum 3$ CTBs in 3C-SiC used in our study is shown Figure 1(b). Table 1 summarizes the geometrical details and process parameters used in the uniaxial tensile and compressive deformation simulations. Note that the realistic strain rates (10^{-4}–10^{0} s^{-1}) are not accessible in MD simulations, and usually high strain rates (10^{6}–10^{9} s^{-1}) are employed which are virtually 10 orders of magnitude different from experimentally-relevant strain rates [34]. In the present study, 10^{9} s^{-1} is selected as an optimal strain rate, in line with other studies [35-37], to run a large set of simulations. Nanotwinned nanocrystalline samples, with the cubic length size of 25 nm, with four mean grain sizes *d* ranging from 4 nm to 15 nm and a CTB spacing λ varying from 1.5 nm to 12 nm are adopted. Twin-free nanocrystals are also examined for the sake of comparison. It is worth noting that large grain samples in the present study contain only a few grains, which consequently may bring about size effects and restrict our results to some specific cases. Two representative simulations were performed for the twin-free and nanotwinned nanocrystals with *d*=12 nm and λ=3 nm using large samples with the cubic length size of 50 nm, containing ~12 million atoms. As shown in Supplementary Figure S1, the samples exhibit size effect, namely the yield stress increases with decreasing sample size, which is about 13% and 11%, respectively, for the twin-free and nanotwinned samples.

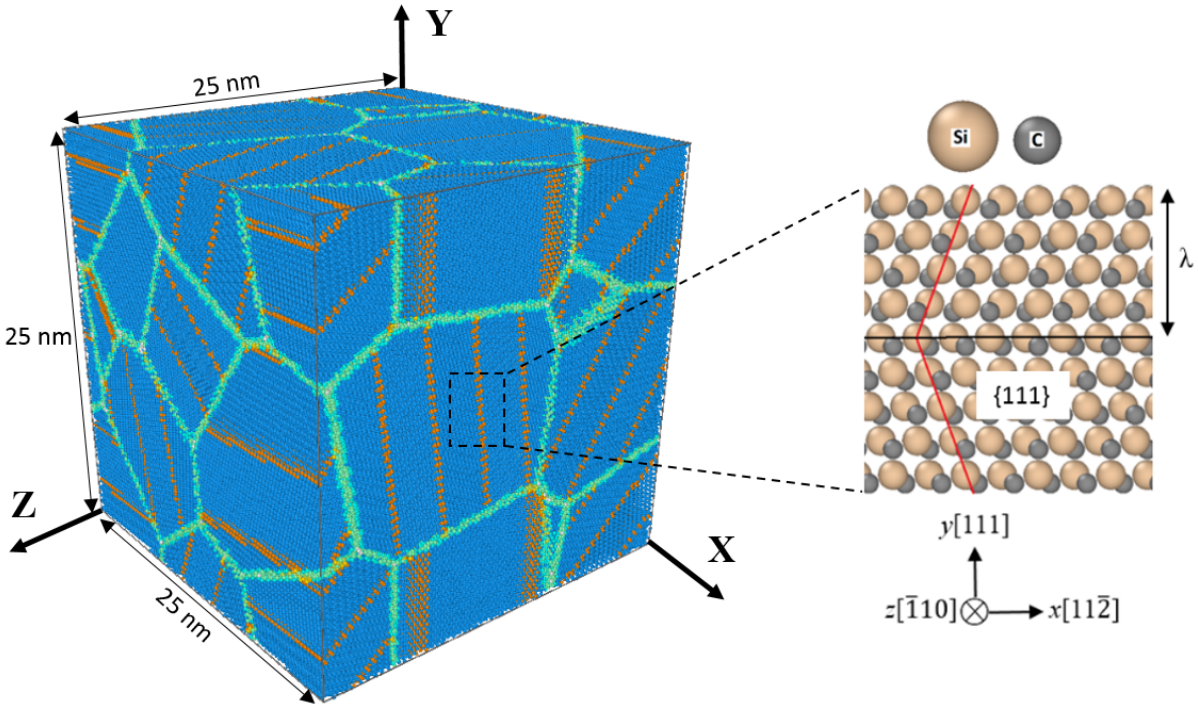

Figure 1 (a) An example of the nanotwinned nanocrystalline 3C-SiC structure after relaxation. Atoms are coloured according to a structure identification algorithm for diamond lattice [33]. Intragranular phase, which is pristine diamond lattice, is represented by blue atoms whilst GBs and CTBs are mainly shown in green and orange colour, respectively. (b) Schematic illustration of the atomic arrangement of {111} ∑3 CTBs in 3C-SiC used in this study.

Periodic boundary conditions are imposed in all directions to reduce the effects of the simulation cell size. To relax the randomly introduced GBs before performing loading simulations, all pairs of atoms at the GBs whose distance of separation is smaller than 0.9 Å are searched for and one of the two atoms is removed, so that the abnormally high atomic density regions at the GBs are eliminated which aids in minimizing the system energy. Then, molecular statics with an ultimate relative energy convergence of 10^{-8}, followed by a dynamic relaxation for 30 ps under isothermal-isobaric (NPT) dynamics at 300 K are performed to relax the system and attain a thermal equilibrium state. It should be mentioned that, as discussed by Rupert and Schuh [38], the way the local structural relaxation of GBs is performed could alter the mechanical behaviour of nanocrystalline material. A few simulations using high-temperature annealing were performed in order to find out whether results would change. Two

representative cases i.e. the twin-free nanocrystal with d=8 nm and nanotwinned nanocrystal with d=12 nm and λ=3 nm were annealed at a high temperature of 2000 K for 30 ps under NPT ensemble. Then, the samples were cooled down to room temperature and subsequently equilibrated at 300 K for 10 ps. Both the samples relaxed by high-temperature annealing exhibited higher compressive strength, ~11%, see Supplementary Figure S2. However, exploring such effects is out of the scope of the current contribution. In our simulations, after relaxation, under an NPT ensemble, uniaxial compressive and tensile loading at constant engineering strain rates is imposed in the Y direction while zero normal stress conditions are prescribed in the X and Z directions at 300 K. Atomic structures are visualized and analysed using OVITO [39].

Table 1 Details of the MD simulations of the uniaxial deformation. λ and d designate the CTB spacing and mean grain size, respectively.

Material systems	Twin-free and nanotwinned nanocrystalline 3C-SiC d: 4, 8, 12, 15 nm λ: 1.5, 3, 6, 8, 12 nm; λ<d
Interatomic potential function	Vashishta [31]
Ensemble	NPT
Time step	1.0 fs
Boundary conditions	Periodic in all directions
Dimension of the sample	25×25×25 nm^3
Number of atoms in the	~ 1.5 millions

sample	
Strain rate	$10^9\ s^{-1}$
Temperature	300 K

III. Results and discussion

A. Twin-free nanocrystal. A typical uniaxial tensile and compressive stress-strain response of the twin-free 3C-SiC nanocrystal is illustrated in Figure 2(a-b), where a clear dependence of the elastic modulus on CTB spacing is discernible. With decreasing grain size from 15 nm to 4 nm, the elastic modulus decreases, exhibiting an 'Inverse Hall-Petch' behaviour at fine grain sizes, in consistent with prior studies in Cu [40]. Further analysis reveals that, under both uniaxial tensile and compressive stress loading, a decrease in grain size is accompanied by a shift from linear to non-linear behaviour in the elastic regime at high strains, typically known as elastic softening. However, elastic hardening is not observed. The observations collectively call attention to the significance of the volume fraction of soft disordered intergranular phase at GBs which essentially govern the material's mechanical response [41]. As evident from Supplementary Figure S3(a-b), as the grain size reduces, the volume fraction of disordered atoms, primarily lying at GBs, increases, culminating in non-linear elastic response and enhancement of the plasticity. Also, the evolution plots show a continuous increase in the volume fraction of disordered atoms with increasing compressive strain, whilst a slight drop occurs after yield/fracture point (beyond the strain of 0.07, which are not shown in Supplementary Figure S3(b)) in uniaxial tensile stress loading of nanocrystals with $d \leq 8$ nm, which could be a consequence of GB relaxation and short-range atom disorder-to-order transition triggered by the release of the elastic strain energy stored in the nanocrystal. Note that careful examination of the simulation snapshots uncovered trivial order-to-disorder

transition of pristine diamond lattice inside grains in some special cases, which will be discussed in the following section.

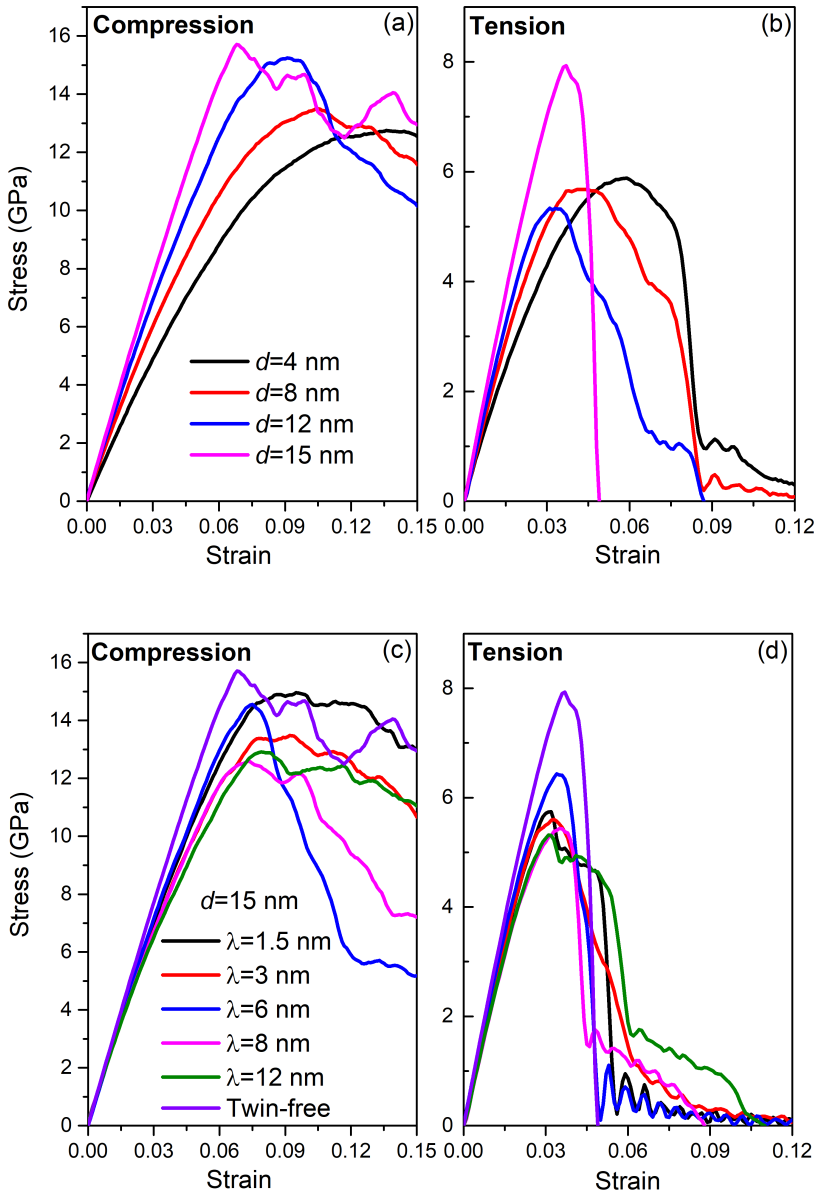

Figure 2 Uniaxial stress-strain behaviour of (a-b) twin-free 3C-SiC nanocrystals with different grain sizes, (c-d) nanotwinned nanocrystalline with d=15 nm at 300 K and strain rate of 10^9 s^{-1}.

The stress-strain curves shown in Figure 2(a-b) also hint at a remarkable brittle-to-ductile transition with decreasing grain size. Under compressive deformation, the 3C-SiC nanocrystal with large grains, of the order of 15 nm, offers low ductility, where a stress drop transpires in

a short interval once the strain reaches its critical value. Under tensile deformation, this nanocrystal fails by a semi-brittle fracture, as demonstrated in Figure 2(b). By monitoring the deformation snapshots, it is perceived that the GB decohesion and crack initiation/propagation along GBs of the nanocrystal with large grains contribute to the observed behaviour. In particular, during uniaxial tensile stress loading, once the crack initiates through the decohesion of GBs, it propagates quickly via cleavage, in a brittle way, without assistance of dislocation activity. During uniaxial compressive stress loading, deformation induces GB migration in the twin-free nanocrystals with large grains, d=15 nm, attributable to the strain accommodation of a few GBs in this nanocrystal relative to the finer grain nanocrystals encompassing more GBs. Dislocation extraction algorithm (DXA) [42] analysis indicates no distinct dislocation activity in the grains during uniaxial tensile deformation of the 3C-SiC nanocrystal, see Supplementary Figure S4(b). Note that diamond cubic 3C-SiC lattice comprises two interpenetrating fcc lattices, which can lead to slips on the four equivalent {111} planes. The preferred slip systems are closely correlated to the core structure of their mobile dislocations. Hence, dislocations have to glide in these planes with the Peierls stress of 7.5 GPa, as estimated by the Peierls-Nabarro model [43]. There exist pre-existing partial and perfect dislocations which are inherently formed during building nanocrystals. Such pre-existing dislocations might reduce the applied stress needed for plastic deformation, yet the crystallographic orientation of the grains in conjunction with the loading direction, along with the high Peierls stress, are the decisive factors for activating such pre-existing dislocations. It is inferred that lattice dislocation nucleation and propagation form the GBs does not take place, and the pre-existing dislocations cannot overcome the Peierls stress during the uniaxial tensile deformation to be activated and migrate, thus, the imposed strain energy is primarily accommodated by the GB-mediated mechanisms, i.e., atomic shuffling, GB sliding, and voiding. The evolution plot of full dislocation density, defined as: full dislocation density = (perfect dislocation line length +

(partial dislocation line length / 2)) / system volume, for the samples under uniaxial tensile deformation shows annihilation of pre-existing dislocations before yielding, and their re-nucleation up to the roughly same level of dislocation density, presumably due to the rearrangement of GB atoms during tension leading to the reduction of GB dislocations, followed by the returning of GB atoms to their initial positions caused by the stress relaxation after tensile yielding/fracture. On the other hand, no immediate trend is visible for the samples under uniaxial compressive deformation, albeit density of full dislocations increases in some cases, i.e., in nanocrystals with d=4 nm and d=12 nm. In these samples, pre-existing dislocations are initially activated at the early stage of deformation, where the critical resolved shear stress of intragranular dislocation differs little depending on the straining direction. Hence, a cooperation of dislocation activity and GB processes is occurred at the initial stage of the uniaxial compressive stress loading up to $\varepsilon = 6\%$; beyond that, mere release of the compressive strain energy by GB-associated processes takes place. Nonetheless, dislocation nucleation transpires in some, not all, of the grains of these nanocrystals, plausibly due to superior crystal orientation, e.g., a higher Schmid factor, than other grains. Note that the activation of lattice dislocation slips does not lead to a macroscopic yield since the plastic strain produced by a few intragranular dislocation motion is trivial.

Under uniaxial deformation, nanocrystals exhibit a softening behaviour below a critical grain size, i.e. $d \leq 8$ nm, signifying an increase in ductility with decreasing grain size. Notice that strain localization via necking is hindered in the samples owing to the bulk geometry. A detailed analysis reveals that during compressive loading, cracking along GBs does not occur for the nanocrystal with very fine grain size, of the order of 4 nm, implying the softening effects of disordered intergranular phase at GBs. Moreover, in fine grain size samples, strain localization is inhibited due to the high activity of GB processes, leading to the slow void growth and coalescence (see Supplementary Figure S5(b)) which culminates in wide local

plasticity and ductile plastic response, as evident in stress-strain curves. Notice that the void formation was analysed through the surface mesh method [44] with the probe sphere radius of 2.5 nm, which is larger than the nearest neighbour atom separation in 3C-SiC nanocrystal (~1.9 nm) obtained by radial distribution function.

B. Nanotwinned nanocrystal. Figure 2(c-d), exemplarily, displays the uniaxial tensile and compressive stress-strain behaviour of the nanotwinned 3C-SiC nanocrystal with d=15 nm. Clearly, twinning has a pronounced influence on the elastic behaviour, strength, and ductility of the 3C-SiC nanocrystals. The elastic modulus of the nanotwinned nanocrystal with d=15 nm is marginally lower than their twin-free counterparts. This specific elastic behaviour is observed for all the studied nanocrystals, however, as the grain size is reduced, the influence of twinning on the elastic properties is less noticeable. The evolution plots of the volume fraction of disordered intergranular phase, see Supplementary Figure S3, indicate that in some cases, e.g., nanotwinned nanocrystal with d=4 nm, a small decrease of the volume fraction of disordered atoms at the initial stage of compressive loading takes place, which accentuates to the short-range atom disorder-to-order transformations. By monitoring the compressive deformation snapshots, a small amount of order-to-disorder transition of diamond lattice lying between CTBs in nanocrystals with $d \geq 8$ nm containing thin nanoscale twins, λ=1.5 nm, is observed before yielding. This particular transition initiates from the GBs, expanding up to approximately half of the grain diameter. In some cases, a reverse transformation after yielding occurs, which corresponds to the stress relaxation.

Figure 3(a-b) shows the representative snapshots of uniaxial compressive and tensile deformation of the nanotwinned nanocrystals with different grain sizes and CTB spacings, i.e. d=15 nm and λ=6 nm, and d=4 nm and λ=1.5 nm, where the locations of crack propagation are illustrated. Evidently, no distinct dislocation activity is visible, and extensive cracking does not transpire in fine grain size samples at the point of yielding/fracture. As seen in Supplementary

Figure S4, in general, the density of pre-existing dislocations in the nanotwinned nanocrystals is lower than their twin-free counterparts, suggesting that the dislocation sources with sufficiently small grains and/or twins cease to operate. The evolution plots of the full dislocation density for the nanotwinned nanocrystals presented in Supplementary Figure S4(c-f) exhibit very interesting trends. During uniaxial compressive stress loading, the dislocation density in the finest grain size sample, d=4 nm, increases up to the strain of 5%, and then it levels off. In these samples, the amount of dislocation density remains unchanged at the point of yielding, implying that at the early stage of straining, imposed strain is accommodated by dislocation slip, followed by mere GB-mediated plasticity. In some other samples with different grain sizes and CTB spacings, this behaviour is also observed. In most cases, the aforementioned plasticity mechanisms, i.e., minor dislocation slip followed by mere intergranular deformation processes at the yield point governs the deformation behaviour of the nanotwinned nanocrystals subjected to uniaxial compressive loading. One striking observation, depicted in Supplementary Figure S4(e), is the sharp rise, approximately fifteen fold, of dislocation density up to the yield point in the nanotwinned nanocrystal with d=12 nm and λ=1.5 nm, signifying that dislocation slip and GB processes cooperate to release the imposed strain energy.

Under uniaxial tensile stress loading, dislocation density in nanotwinned samples with $d \geq 12$ nm exhibit monotonic decrease; the drop is more pronounced for the large grain size sample, d=15 nm. In the samples with finer grain sizes, dislocation density starts to decrease before yielding/fracture, and then it increases. The trend is perceived to be non-linear. Note that the dislocation density in nanotwinned nanocrystals with $d \leq 12$ nm and λ=1.5 nm remains relatively constant up to the yield point. On the basis of the above argument, it is suggested, generally, that lattice dislocation slip does not contribute to the deformation of the nanotwinned nanocrystal samples subjected to the tensile loading. We remark that similar to their twin-free

counterparts, a small decrease of the fraction of disordered atoms occurs after yielding/fracture in uniaxial tensile stress loading of nanotwinned nanocrystals with $d \leq 8$ nm.

During tensile and compressive deformation of nanotwinned nanocrystalline 3C-SiC samples with large grains, mainly intergranular crack propagation and fracture transpires along the GBs but not the CTBs, which can be explained by the GB and CTB energies of 3C-SiC predicted by the Vashishta potential. The calculated normalized GB energy per atom is 0.224 eV, which is much higher than its normalized CTB energy per atom of 0.014 eV, suggesting the propensity of crack formation and extension along a high-excess-energy intergranular path. However, in some distinct cases, e.g., nanotwinned nanocrystal with d=12 nm and λ=1.5 nm, intragranular crack formation and fracture across CTBs transpires at high strains, after reaching to the yield stress, i.e., in the softening area of the stress-strain curve. As shown in the successive simulation snapshots of Figure 3(c) and Supplementary Movie 1, emission of first individual perfect dislocation slip from GBs occurs at the strain of ~10.6%. As the strain increases, more perfect and partial dislocations are nucleated from GBs and slip along the CTBs inside the grain. Such dislocation activity is attributed to the shear-induced fracture inside the grain. Indeed, the intragranular fracture in our simulations is mediated by the shear-induced cracking with an angle of 45 degree relative to the loading direction, followed by generation and expansion of the Shockley partials with Burgers vector of $\boldsymbol{b} = \frac{1}{6} < 112 >$ along the CTBs, and the contribution of other partial and perfect dislocations. Shear-induced cracking and dislocation motion along the CTBs bring about the generation of CTB steps and subsequent twin plane migration which ruins the coherency of the CTBs, resulting in local sites of stress concentration along them. In this sample, i.e. nanotwinned nanocrystal with d=12 nm and λ=1.5 nm, dislocation emission from GBs expanding along CTBs is also visible in some other grains. Crack deflection from an intergranular path to an intragranular one has also been observed in quasi-3D columnar nanocrystalline Ni [45].

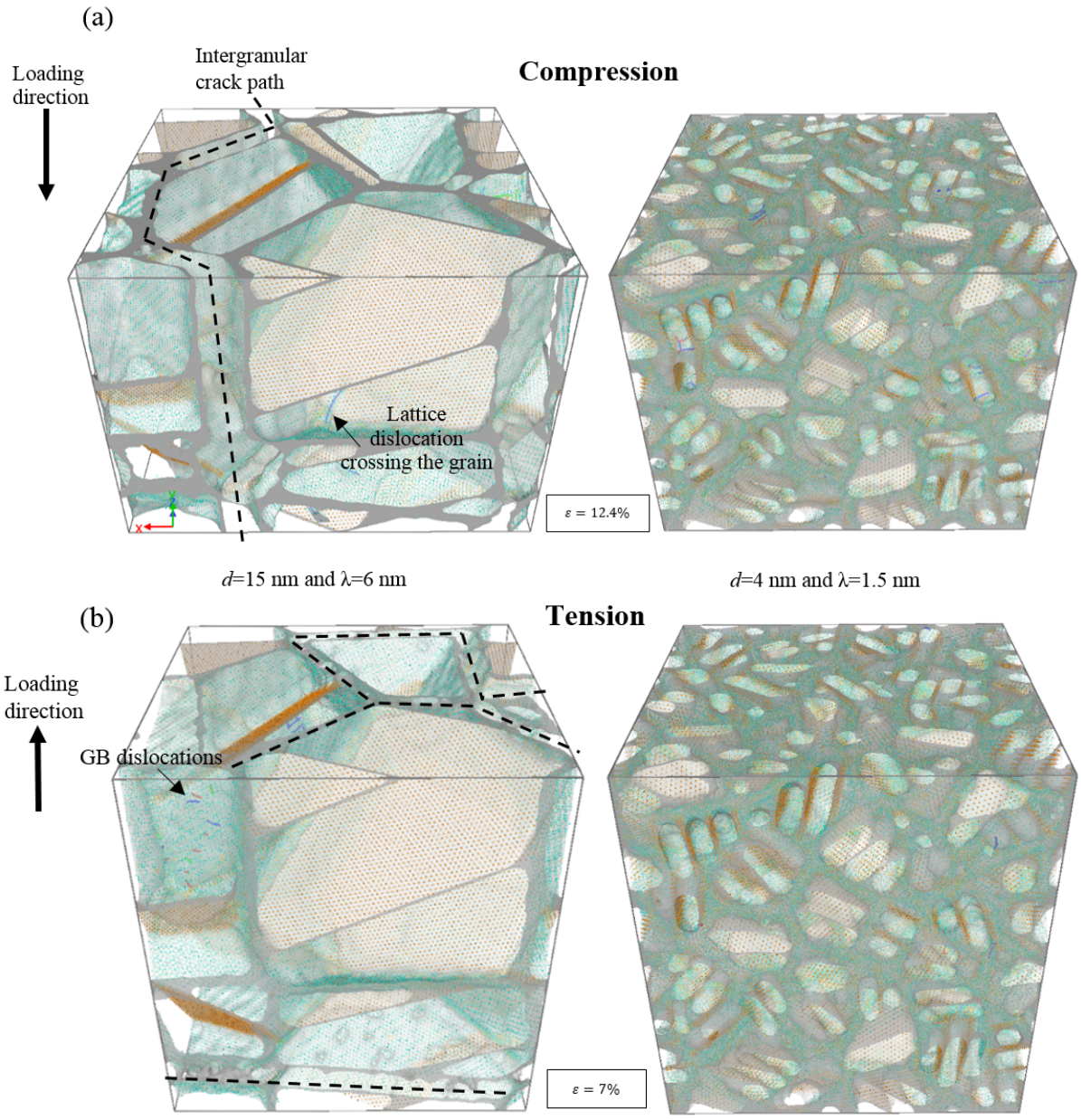
(a)
Loading direction
Intergranular crack path
Compression
Lattice dislocation crossing the grain
ε = 12.4%
d=15 nm and λ=6 nm
d=4 nm and λ=1.5 nm
(b)
Tension
Loading direction
GB dislocations
ε = 7%

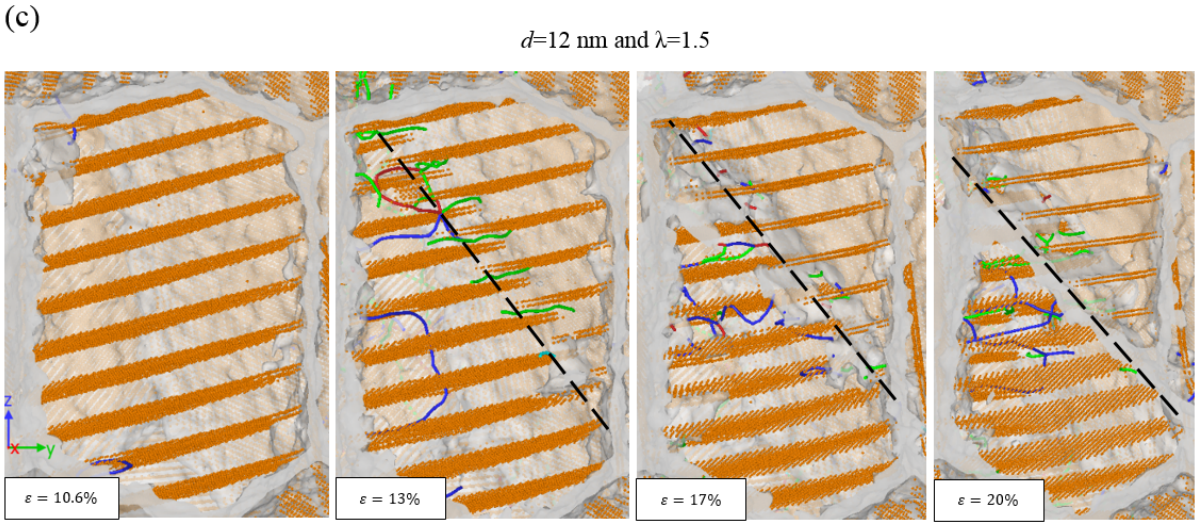
(c)
d=12 nm and λ=1.5
ε = 10.6%
ε = 13%
ε = 17%
ε = 20%

Figure 3 (a-b) Defect structure of nanotwinned nanocrystals subjected to uniaxial compressive and tensile stress loading, (c) The process of shear-induced intragranular fracture, which is also shown in Supplementary Movie 1. Atoms in orange colour designate the CTBs whilst blue, green, aqua, and red lines, respectively, represent the perfect, Shockley partial, Frank partial, and other partial dislocations. The dash lines show the fracture path.

C. Origins of the differences in the mechanical response. To further evaluate the disparities in the mechanical response of the twin-free and nanotwinned nanocrystals, the values of the yield strength (peak stress) and corresponding yield strain of all the samples are extracted from the stress-strain curves and illustrated in Figure 4. As demonstrated in Figure 4(a), the compressive strength of the twin-free sample decreases with grain size, which is known as the Inverse Hall-Petch behaviour, whereas under uniaxial tensile stress loading, strength decreases substantially with decreasing grain size from 15 nm to 12 nm, and then it slightly increases. To characterize such strengthening and softening features, samples are analysed in terms of dislocation density, voiding, disordered intergranular phase, and total strain energy. The values of the aforementioned factors at the point of yielding/fracture are extracted from the evolution plots given in Supplementary Material, and presented in Figures 5-8. Note that the total strain energy is calculated via subtraction of the recorded instantaneous energy of the system from that of the initial energy of the relaxed undeformed system. As evident from the figures, the fraction of the disordered intergranular phase, voids, and total strain energy at the yield point increases with decreasing grain size in twin-free samples. Dislocation density approximately remains constant for $d \leq 12$ nm, followed by an increase in nanocrystal with d=15 nm, during compressive loading whilst during tensile loading, it shows a stochastic behaviour. Ostensibly, lower fraction of disordered intergranular phase, voids, and dislocation density contribute to stiffer response of the 3C-SiC nanocrystals. On the other hand, the lower total strain energy at the yield point could point to the minor portion of GBs in accommodating strain and absorbing energy. Thus, GBs possess lower energy which in turn might result in the suppression of the GB-mediated processes, e.g., atomic shuffling and GB sliding, leading to harder response of

the 3C-SiC nanocrystals. Nevertheless, it should be mentioned here that GB energy alone cannot determine whether/how sliding of nanoscale high-angle boundaries takes place when no thermally activated mechanisms are involved [46]. On the other hand, strengthening may scale with the average atomic energy of the system [38]. Also, note that clean separation of the energy of internal interfaces, i.e., GBs and CTBs, from the strain energy is very difficult, and we do not intend to focus on this issue in the current study. The energy-strain curves in Supplementary Figure S6 show that for the finest grain sizes, the strain energy constantly increases with the strain, below and beyond the yield point, however, in larger grains, it grows slowly, levels off, and decreases beyond the yield point.

It appears that minor movements of GB dislocations and nucleation of embryonic partial dislocations inside some grains do not influence the mechanical response of the twin-free nanocrystals subjected to uniaxial compressive stress loading. Thus, it is assumed the strength is merely governed by the disordered intergranular phase, voiding, and energy of GBs. On the other hand, the response of the twin-free sample under uniaxial tensile stress loading shows a turning point at the grain size of 12 nm, implying that the tensile strength of the fine grain nanocrystals does not purely rely on the voiding, disordered intergranular phase, dislocation density, and energy of GBs. It can be postulated that structural characteristics, e.g., GB and triple junction area distribution normal to the straining direction, decohesion strength of randomly distributed GBs associated with GB structure, and dissimilar number of neighbours per grain cause different stress distributions in the microstructures, which determines the macroscopic tensile response of the twin-free nanocrystals with $d \leq 12$ nm. However, in nanocrystals with large grains, $d > 12$ nm, fraction of disordered intergranular phase and voids are the main controlling mechanisms. Figure 4(b) and Figure 4(d) confirm that the ductility of twin-free nanocrystals follows the identical trend observed for the yield strength. Under compressive loading, strengthening nanocrystalline 3C-SiC by increasing the grain size comes

at the expense of lowering the ductility, with strain-to-yield values of 0.136 and 0.068 observed for the grain sizes of 4 nm and 15 nm, respectively. Under tensile loading, the strain-to-yield value is first reduced from 0.059 to 0.031, followed by a slight increase to 0.037. In general, it can be assumed that more GBs carry plastic deformation in nanocrystals with fine grains, thus, strain distribution is more uniform, resulting in high ductility. The influence of uniform distribution of imposed strain in fine grains can be also seen in terms of the tensile yield strength, Figure 4c, where fine grain nanocrystals with d=4 nm exhibit slightly higher strengths.

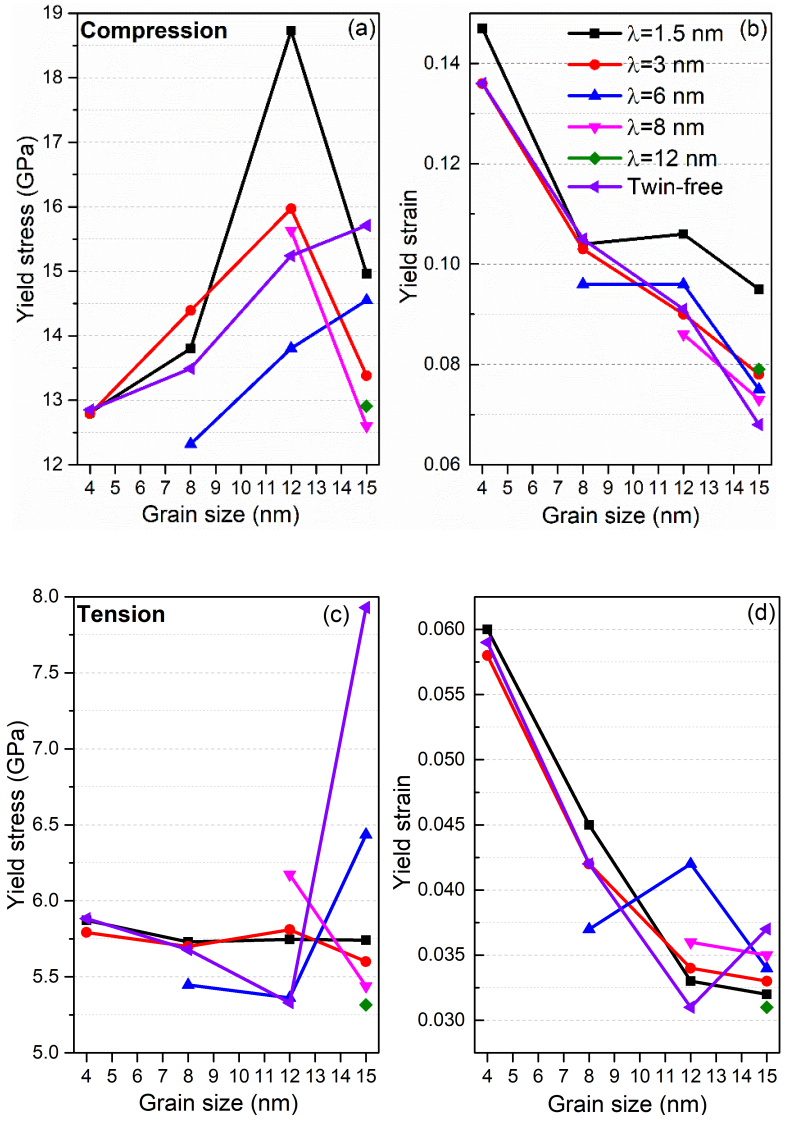

Figure 4 (a-b) Compressive and (c-d) tensile yield strength and yield strain as a function of grain size and CTB spacing λ.

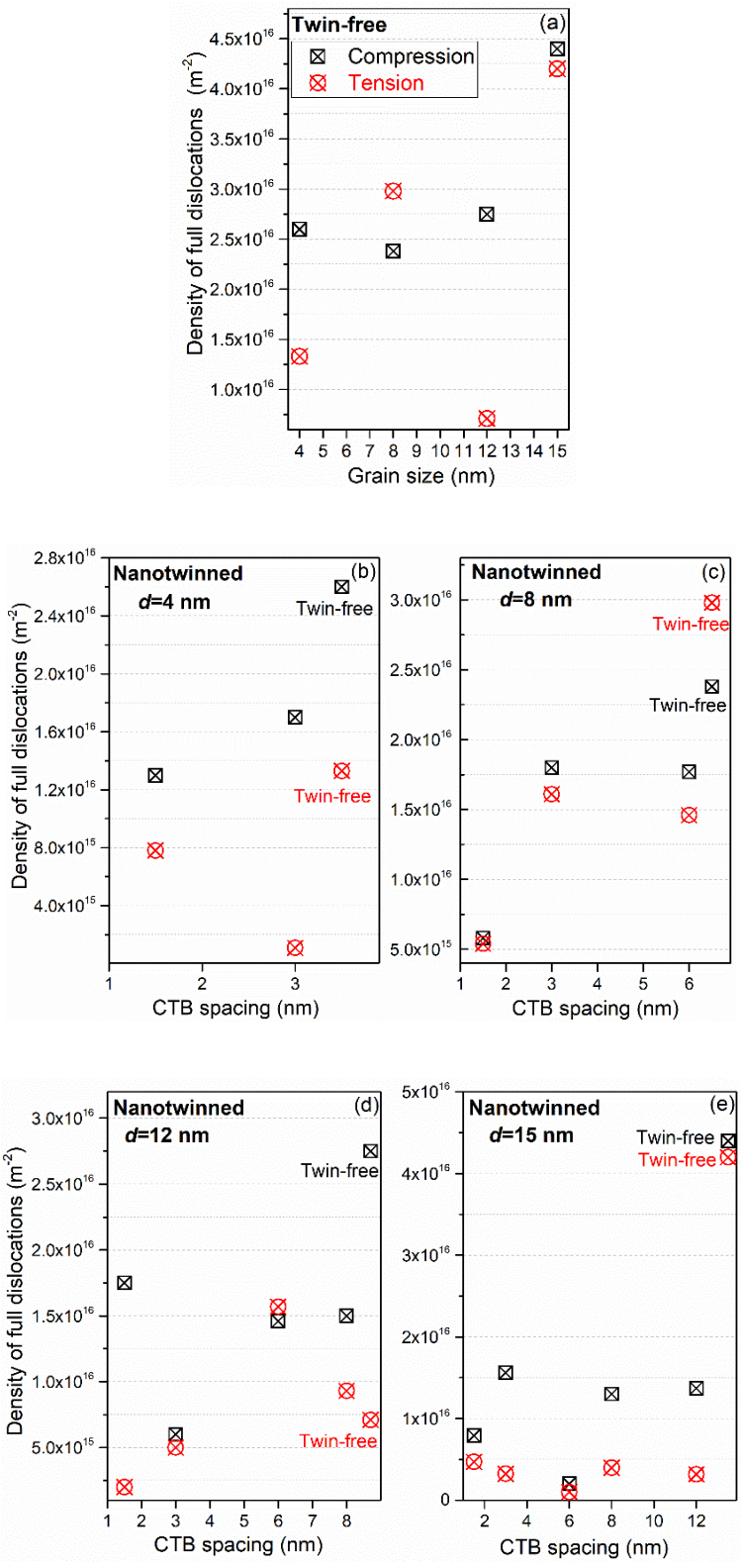

Figure 5 Density of full dislocations at the point of yielding/fracture as a function of grain size and CTB spacing; (a) Twin-free and (b-e) nanotwinned samples subjected to uniaxial compressive and tensile stress loading.

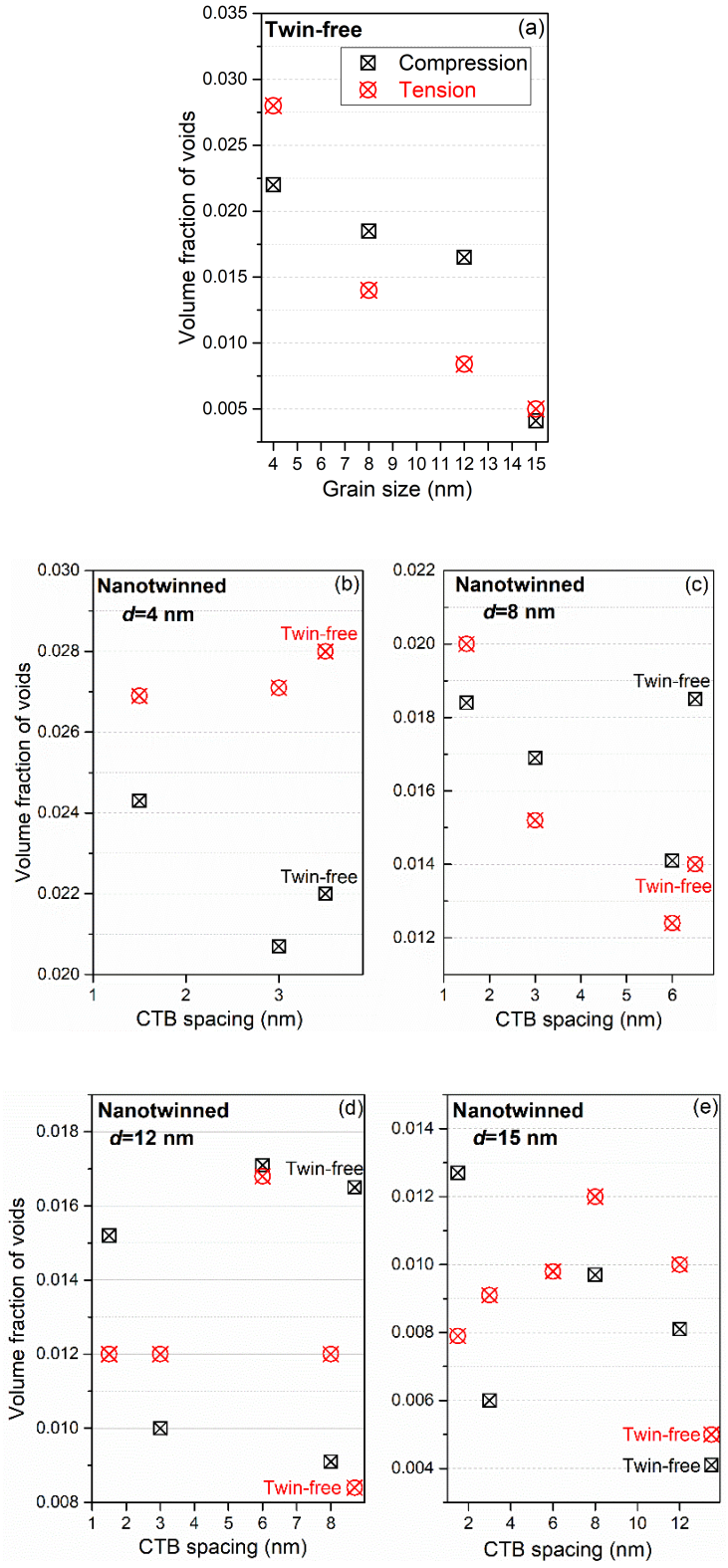

Figure 6 Volume fraction of voids at the point of yielding/fracture as a function of grain size and CTB spacing. (a) Twin-free and (b-e) nanotwinned samples subjected to uniaxial compressive and tensile stress loading.

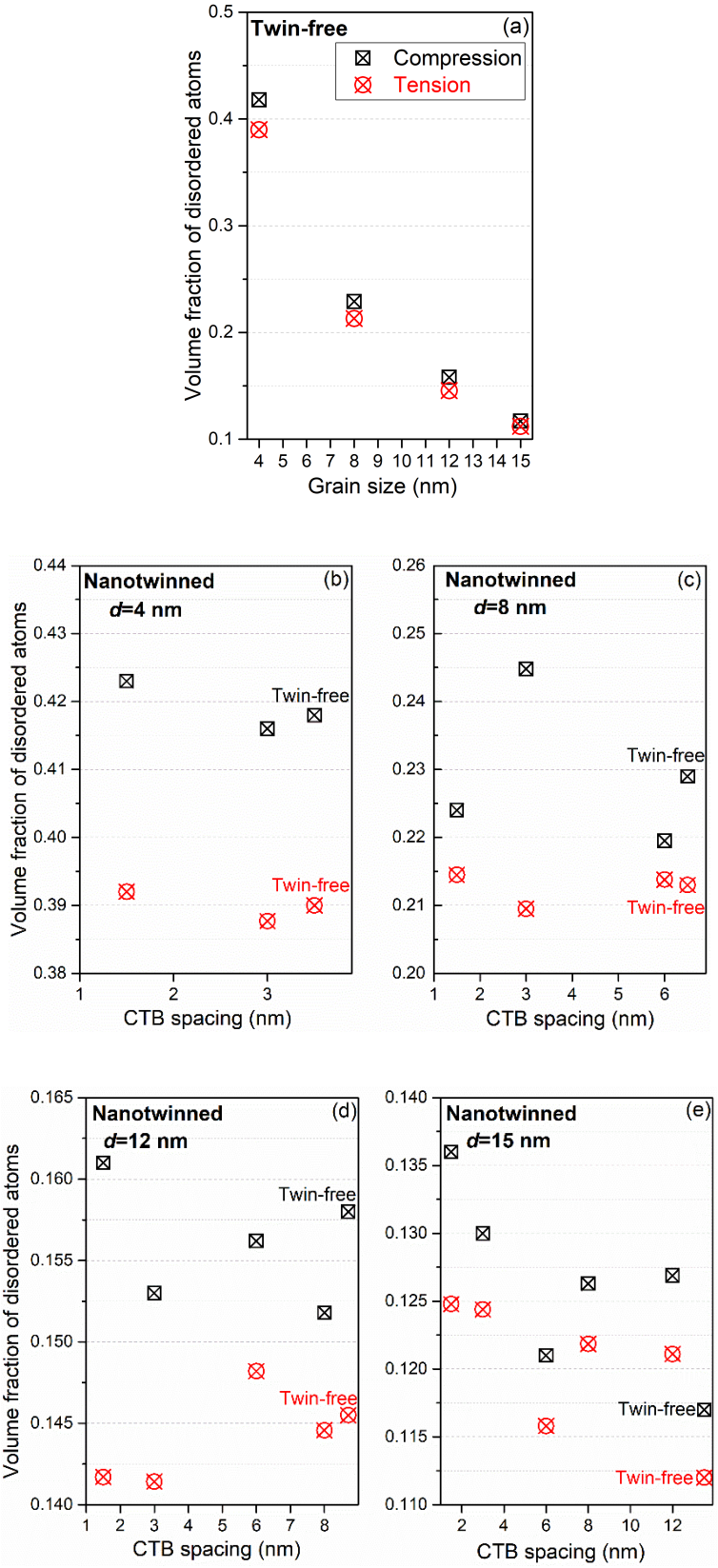

Figure 7 Volume fraction of disordered atoms, mainly lying at GBs, at the point of yielding/fracture as a function of grain size and CTB spacing. (a) Twin-free and (b-e) nanotwinned samples subjected to uniaxial compressive and tensile stress loading.

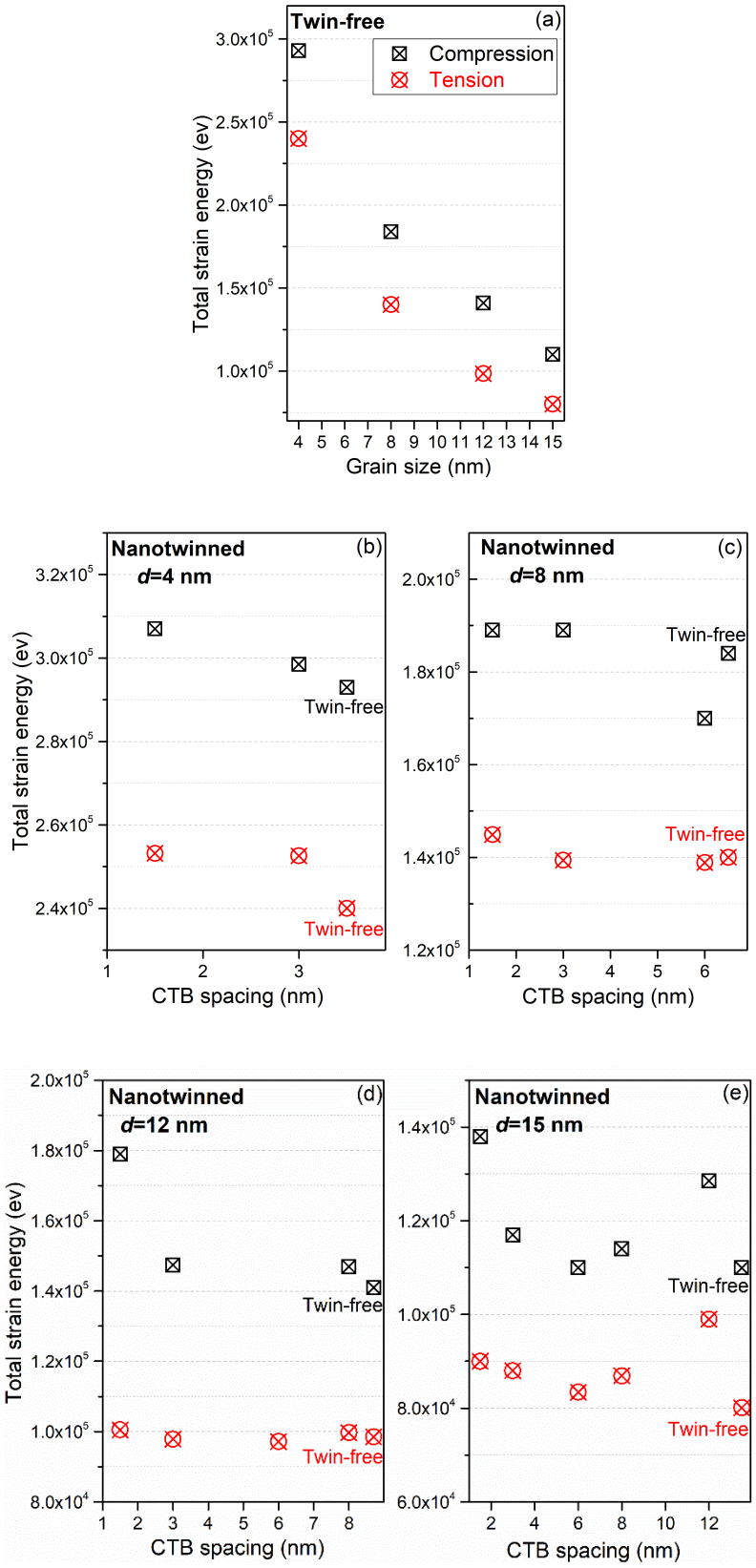

Figure 8 Total strain energy at the point of yielding/fracture as a function of grain size and CTB spacing. (a) Twin-free and (b-e) nanotwinned samples subjected to uniaxial compressive and tensile stress loading.

Figure 4 shows that embedding nanoscale twins in the nanocrystals can induce interesting effects on the yield strength and ductility of the samples. The twinning effects are more pronounced under compressive deformation than tensile loading. As shown in Figure 4(a), the twinning effects on the compressive strength increase with the grain size. Moreover, for each grain size, there is a specific density of CTBs at which the strength is maximum. However, on account of scatter in the data, no firm trend for the strength with CTB spacing and grain size can be drawn. Compressive strength of the twin-free and nanotwinned nanocrystalline samples with d=4 nm is ~12.8 GPa, suggesting that twinning has no effect on the strength of the finest grain size samples. Further investigation of the compressive strength of samples with varying twin thickness reveals that compressive strength behaviour of the all nanotwinned 3C-SiC nanocrystals cannot be systematically explained by the deformation features such as dislocation density, voiding, disordered intergranular phase, and total strain energy. For instance, in nanotwinned nanocrystals with d=8 nm, although the volume fraction of disordered intergranular phase and voids are the lowest in the sample with λ=6 nm (Figure 6(c) and Figure 7(c)) compared with others with different λ, its strength is the lowest. Note that the total strain energy incorporates the energies of internal interfaces, i.e. GBs and CTBs. Nevertheless, since the energy of GBs is much higher than that of the CTBs in 3C-SiC nanocrystals, and because of the disparate distribution of GBs and CTBs in different samples, the total energy of internal interfaces predominantly represents the energy of GBs in the nanocrystals. In such case, the total strain energy may be used as a measure to mainly assess the capability of GBs in accommodating strain and absorbing energy. In the nanotwinned nanocrystal with d=12 nm and λ=6 nm, the total strain energy is the lowest compared to other samples with the same d but different λ, plausibly indicative of low contribution of GBs and twin planes in the load-bearing process, which may lead to the low strength and ductility. Figure 4(b) indicates that under compressive loading, good ductility is preserved while inserting a high density of twins,

λ=1.5 nm, into the grains, probably originating from the strain accommodation and energy absorption by the GBs and dense twin planes. In general, for the grain sizes $d > 8$ nm, twinning effects on the ductility is more pronounced. A plateau region is observed for some specific grain sizes and CTB spacings. Slope of the plots shows that nanoscale twins impact the nanocrystalline material's ductility more markedly when the grain size is small, $d < 8$ nm, than those of coarse ones with $d > 12$ nm. In the case of the nanocrystal with *d*=4 nm and λ=1.5 nm, see Figure 7(b) and Figure 8(b), the disordered intergranular phase and total strain energy are the highest among all nanocrystals with *d*=4 nm, suggesting a high ductility. As illustrated in Figure 7(c) and Figure 8(c), in nanocrystal with *d*=8 nm, the volume fraction of the disordered intergranular phase and total strain energy are minimum for the sample with λ=6 nm, which could signify a low ductility, see Figure 4(b). Similarly, as depicted in Figure 7(d) and Figure 8(d), in nanocrystals with *d*=12 nm, the volume fraction of the disordered atoms and the total strain energy is the lowest for the sample with λ=8 nm, prompting the lowest ductility in this nanocrystal. In the case of nanocrystal with *d*=12 nm and λ=1.5 nm, as seen in Supplementary Figure S4(e), the dislocation activity is intense, causing the dislocation-CTB interaction which provides ample local sites for dislocation accommodation. Such interactions could also give rise to the enhancement of ductility in this sample. Figure 7(e) and Figure 8(e) demonstrate that the lowest volume fraction of the disordered intergranular phase and total strain energy in nanocrystals with *d*=15 nm transpires for the twin-free sample, in consistent with the observed minimum ductility for these nanocrystals in Figure 4(b).

Another remarkable point is that, aside from the samples with λ=6 nm, the combination of grain size and CTB spacing shows a Hall-Petch-like behaviour, i.e., the compressive strength first increases with decreasing grain size, reaching a maximum at a critical value (*d*=12 nm), and then constantly decreases with further refining the grains. The turning point is attained at the grain size of 12 nm. The maximum strength is obtained for the nanotwinned nanocrystal with

d=12 nm and λ=1.5 nm, which is ~23% and ~17%, respectively, higher than its twin-free counterpart with the same *d* and the nanotwinned nanocrystal with *d*=12 nm and λ=3 nm. It must be noted here that the deformation of nanotwinned 3C-SiC nanocrystals is complicated, and numerous factors affect the strength of these nanostructures, including disparate structural characteristics, e.g., GB and triple junction area distribution along/normal to the straining direction, decohesion strength of randomly distributed GBs, dissimilar number of neighbours per grain, crystallographic orientation of grains, and distribution of CTBs inside grains. These factors influence the deformation features such as atom disordering, voiding and its distribution and coalescence, dislocation slipping, energy-related issues of GBs and CTBs, and their capability to accommodate strain and absorb energy, which may operate either sequentially or concurrently, triggering different stress distributions in the microstructures. According to such complex interplay, intricate deformation paths and yielding morphologies occur which makes it difficult to come up with a single mechanism for the observed behaviours. However, we assume that GB and triple junction area distribution along/normal to the straining direction and capability of CTBs to accommodate strain and absorb energy are the most effective factors on the strength and ductility of nanotwinned nanocrystals. For example, a close examination of the deformation snapshots for the nanocrystal with *d*=12 nm and λ=1.5 nm and λ=6 nm, shown in Figure 9, subjected to uniaxial compressive stress loading reveals that GB and triple junction distribution in the sample with λ=6 nm is in such a way that more GBs are available along the straining direction (*Y*) than that of the sample with λ=1.5 nm, causing the initiation of a vast transvers crack mediated by shear stress concentration at GBs, which consequently lowers the strength of the nanocrystal. As palpable from Figure 9(a), GBs which are near perpendicular to the crack propagation direction can act as effective barriers to crack extension. Some GBs normal to the *Y* (in *X*) direction are seen to thicken due to order-to-disorder transition of atoms adjacent to GBs triggered by the applied compressive stress. Careful inspection of the location

of cracks shows that density of the pre-existing GB dislocations, which can ruin and weaken the GBs, is not influential in the place of crack initiation in 3C-SiC nanocrystals. This is different from the crack formation by Zener-Stroh mechanism [47, 48] observed in nanocrystalline tantalum [9]. In the same way, during uniaxial tensile stress loading, the structural characteristics are the determining factor, where fracture is initiated at GBs perpendicular to the loading direction.

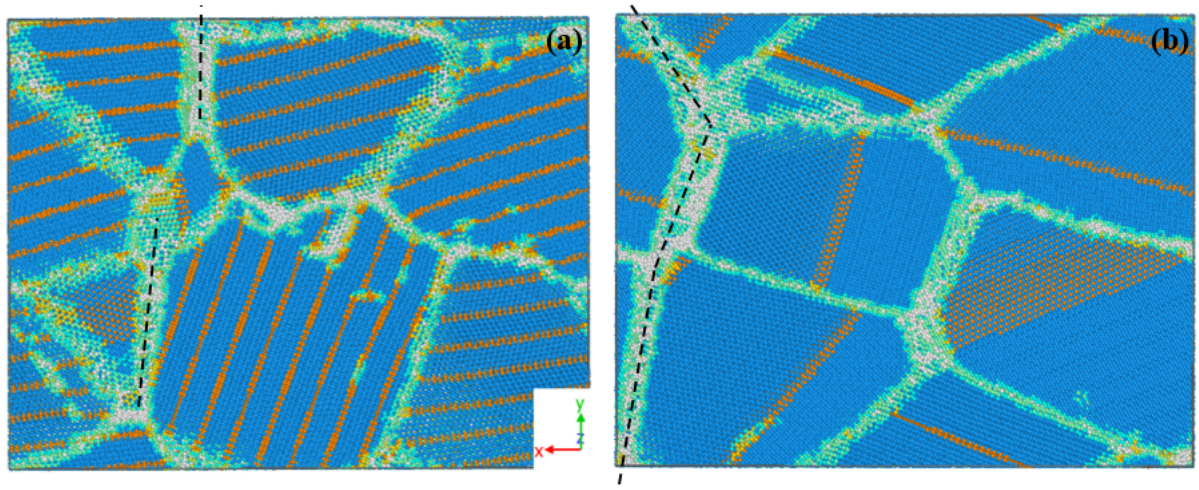

Figure 9 Nanotwinned nanocrystals with (a) d=12 nm and λ=1.5 nm (b) d=12 nm and λ=6 nm, subjected to uniaxial compressive stress loading. GBs area and triple junctions along the straining direction (Y) greatly affect the strength of the nanocrystals.

As depicted in Figure 4(c), twinning does not influence the strength of 3C-SiC nanocrystals with λ ≤3 nm under uniaxial tensile deformation. Thus, their tensile strength remains at ~5.8 GPa. Similar to the uniaxial compressive stress loading, the twinning effect on the tensile strength is more marked for larger grain sizes. Since the tensile failure initiates preferentially at GBs normal to the applied strain direction, the tensile failure is profoundly dependent on the structural characteristics, e.g., GB area distribution normal to the straining direction and decohesion strength of the GBs. Thus, once again, we presume that the measures of the

deformation features cannot provide a comprehensive explanation for our observations, and some inconsistencies may be observed. This conjecture can be verified by examining the volume fraction of disordered atoms, voids, dislocation density, and total strain energy. Figure 6(c) shows that while the volume fraction of voids is the lowest in the nanocrystal with *d*=8 nm and λ=6 nm, it exhibits the minimum strength. On the other hand, the total strain energy is the lowest as well, confirming the low accommodation of strain by the GBs and CTBs in this case. In nanocrystal with *d*=12 nm and λ=6 nm, the volume fraction of the disordered intergranular phase, voids, and dislocation density is the highest, suggesting a low strength. However, while the total strain energy is the lowest for this sample, it exhibits the highest ductility relative to other samples with the same *d*, see Figure 4(d), plausibly due to the high level of dislocation activity. As demonstrated in Figure 6(e) and Figure 7(e), in nanocrystals with *d*=15 nm, the volume fraction of the disordered atoms and dislocation density is the highest whilst the volume fraction of the voids is the lowest and the strain energy is relatively high for the sample with λ=1.5 nm. This sample shows a low tensile ductility and moderate strength. By and large, the variation of the tensile strength in the nanotwinned nanocrystals is ~17%, with maximum and minimum strengths of 6.4 GPa and 5.3 GPa, respectively, in samples with *d*=12 nm and λ=6 nm, *d*=15 nm and λ=12 nm. The significance of the twins in attaining higher ductility is supported by a slight increase in tensile ductility for the samples with $d \leq 12$ nm, see Figure 4(d). Nevertheless, some discrepancies are observed in the trend, which can be ascribed to the GB area and decohesion issues.

D. T-C asymmetry in the strength. The stress-strain curves and plots shown in Figure 2 and Figure 4 present a clear T-C asymmetry in the strength of diamond 3C-SiC nanocrystals, which is much stronger than those in fcc metals [6-8, 13, 49-51]. To further quantify the T-C asymmetry in 3C-SiC nanocrystals, the degree of T-C asymmetry is defined as $(\sigma_Y^C - \sigma_Y^T)/(\sigma_Y^C + \sigma_Y^T)$, where σ_Y^C and σ_Y^T represent yield stress in compression and tension, respectively [52]. Figure

10 illustrates how the degree of T-C asymmetry changes with the grain size and CTB spacing. For all the cases, the degree of T-C asymmetry varies between ~0.33 to ~0.53, which is much higher than those in UFG Cu, ~0.04, and UFG Al, ~0.08 [52]. As indicated previously, the strength in compression is noticeably larger than that in tension, leading to a strong T-C asymmetry in 3C-SiC ceramic. The disparity in T-C asymmetry is mainly attributed to the failure as a result of GB decohesion and crack propagation via cleavage in the 3C-SiC nanocrystals during uniaxial tensile deformation. However, in fcc metals, dislocation nucleation from GBs primarily controls the plasticity during both tension and compression, leading to a low degree of T-C asymmetry. In twin-free 3C-SiC nanocrystals, the T-C asymmetry in the strength increases with decreasing grain size, and then it constantly drops. On the other hand, twinning imposes diverse impacts on the T-C asymmetry of the nanocrystals. It is rather difficult to draw a general trend for the variation of T-C asymmetry as a function of CTB spacing due to different governing deformation/failure mechanisms, as discussed in the previous section. It can be claimed that in large grain sizes, $d \geq 12$ nm, the highest T-C asymmetry occurs for the thinnest twins. In fine grain sizes, $d \leq 8$ nm, the T-C asymmetry increases with CTB spacing up to λ=3 nm; however, in large grain sizes, $d \geq 12$ nm, the T-C asymmetry decreases with increasing CTB spacing up to λ=6 nm. Another interesting observation is the occurrence of the lowest T-C asymmetry in fine grain samples, irrespective of λ, while the highest happens in large grain sizes.

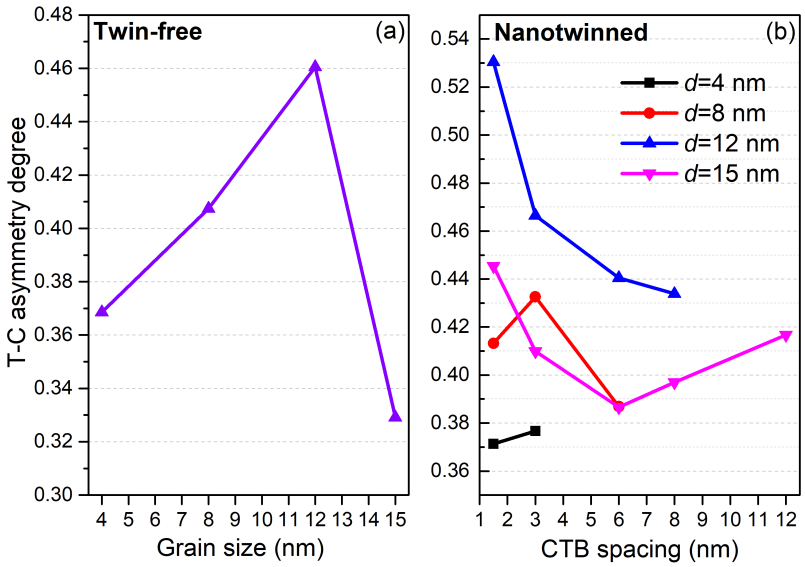

Figure 10 T-C asymmetry in strength of (a) twin-free and (b) nanotwinned nanocrystals as a function of grain size and CTB spacing.

IV. Conclusions

Molecular dynamics simulation observations on tensile and compressive deformation behaviour of nanocrystalline 3C-SiC unravel an intricate interplay of operative deformation mechanisms. This scenario is supported by exploiting the evolutions of voids, intergranular disordered phase, dislocation density, and strain energy during straining as a function of yield strength and ductility. We demonstrate that strength and ductility of nanotwinned samples cannot be exclusively described by any of the individual aforementioned factor; rather, structural characteristics, e.g., GB and triple junction area distribution along/normal to the straining direction, decohesion strength of randomly distributed GBs, dissimilar number of neighbours per grain, crystallographic orientation of grains, and distribution of CTBs inside grains greatly influence material response. Our observations underscore the critical roles of GB and triple junction area distribution along/normal to the straining direction and the capability of GBs and CTBs to accommodate plastic strain and absorb energy. In terms of active plasticity mechanisms, in most cases under uniaxial compressive stress loading, minor dislocation slip

followed by mere intergranular deformation processes at the yield point govern the deformation behaviour of the nanocrystals whilst under tensile loading, nanocrystals are deformed almost exclusively via GB-mediated deformation mechanisms. We also find that mainly intergranular crack propagation and fracture along the GBs occurs, attributable to the high energy of the GBs relative to CTBs. Nonetheless, a high density of nanoscale twins can deflect the crack path from intergranular to intragranular at high strains, beyond the yield point, induced by shear, which triggers the formation of Shockley partial dislocation slip, CTB steps, and twin plane migration. The results also suggest a very strong T-C asymmetry with complicated behaviour, associated with the dominant complex deformation/failure mechanisms.

Supplementary Material

See supplementary material for the (1) effect of the relaxation methodology of GBs on the yield strength, (2) size effects, (3) evolution plots of disordered intergranular phase, dislocation density, voids, and total strain energy, (4) a movie showing the process of intragranular fracture induced by shear in the nanotwinned nanocrystal with d=12 nm and λ=1.5 nm.

Acknowledgements

SZC would like to express his sincere gratitude for the financial support from the BIAM-Imperial Centre for Materials Characterisation, Processing and Modelling at Imperial College London. SZC also acknowledges the use of High Performance Computing (HPC) facilities at Imperial College London. The work of SX was supported in part by the Elings Prize Fellowship in Science offered by the California NanoSystems Institute (CNSI) on the UC Santa Barbara campus. SX also acknowledges support from the Center for Scientific Computing from the CNSI, MRL: an NSF MRSEC (DMR-1121053). This work used the Extreme Science and Engineering Discovery Environment (XSEDE), which is supported by National Science Foundation grant number ACI-1053575.

References

1. X. Li, Y. Wei, L. Lu, K. Lu, and H. Gao: Dislocation nucleation governed softening and maximum strength in nano-twinned metals. Nature. **464**, 877 (2010).
2. S. Xu, J.K. Startt, T.G. Payne, C.S. Deo, and D.L. McDowell: Size-dependent plastic deformation of twinned nanopillars in body-centered cubic tungsten. Journal of Applied Physics. **121**, 175101 (2017).
3. S. Xu and S.Z. Chavoshi: Uniaxial deformation of nanotwinned nanotubes in body-centered cubic tungsten. Current Applied Physics. **18**, 114-121 (2018).
4. S. Xu, S.Z. Chavoshi, and Y. Su: Deformation Mechanisms in Nanotwinned Tungsten Nanopillars: Effects of Coherent Twin Boundary Spacing. physica status solidi (RRL)-Rapid Research Letters. (2018).
5. L. Zhang, C. Lu, K. Tieu, G. Michal, J. Zhang, and G. Deng: Tension/compression asymmetry of grain boundaries with non-planar structure. Materials Research Express. **3**, 085025 (2016).
6. S. Cheng, J. Spencer, and W. Milligan: Strength and tension/compression asymmetry in nanostructured and ultrafine-grain metals. Acta Materialia. **51**, 4505-4518 (2003).
7. A.C. Lund, T. Nieh, and C. Schuh: Tension/compression strength asymmetry in a simulated nanocrystalline metal. Physical Review B. **69**, 012101 (2004).
8. A. Lund and C. Schuh: Strength asymmetry in nanocrystalline metals under multiaxial loading. Acta materialia. **53**, 3193-3205 (2005).
9. Y. Tang, E.M. Bringa, and M.A. Meyers: Inverse Hall–Petch relationship in nanocrystalline tantalum. Materials Science and Engineering: A. **580**, 414-426 (2013).
10. V. Tomar and M. Zhou: Tension-compression strength asymmetry of nanocrystalline α-Fe 2 O 3+ fcc-Al ceramic-metal composites. Applied physics letters. **88**, 233107 (2006).
11. M. Tschopp, G. Tucker, and D. McDowell: Atomistic simulations of tension–compression asymmetry in dislocation nucleation for copper grain boundaries. Computational Materials Science. **44**, 351-362 (2008).
12. G.J. Tucker and S.M. Foiles: Quantifying the influence of twin boundaries on the deformation of nanocrystalline copper using atomistic simulations. International Journal of Plasticity. **65**, 191-205 (2015).
13. F. Zhang and J. Zhou: Tension-compression asymmetry and twin boundaries spacings effects in polycrystalline Ni nanowires. Journal of Applied Physics. **120**, 044303 (2016).
14. X. Li, S. Yin, S.H. Oh, and H. Gao: Hardening and toughening mechanisms in nanotwinned ceramics. Scripta Materialia. **133**, 105-112 (2017).
15. S.Z. Chavoshi and X. Luo: Atomic-scale characterization of occurring phenomena during hot nanometric cutting of single crystal 3C–SiC. RSC Advances. **6**, 71409-71424 (2016).
16. S.Z. Chavoshi and X. Luo: Molecular dynamics simulation study of deformation mechanisms in 3C–SiC during nanometric cutting at elevated temperatures. Materials Science and Engineering: A. **654**, 400-417 (2016).
17. S.Z. Chavoshi and S. Xu: Twinning effects in the single/nanocrystalline cubic silicon carbide subjected to nanoindentation loading. Submitted. (2018).
18. P.S. Branicio, J. Zhang, J.P. Rino, A. Nakano, R.K. Kalia, and P. Vashishta: Shock-induced microstructural response of mono-and nanocrystalline SiC ceramics. Journal of Applied Physics. **123**, 145902 (2018).
19. P.S. Branicio, J. Zhang, J.P. Rino, A. Nakano, R.K. Kalia, and P. Vashishta: Plane shock loading on mono-and nano-crystalline silicon carbide. Applied Physics Letters. **112**, 111909 (2018).
20. S.Z. Chavoshi, S.C. Gallo, H. Dong, and X. Luo: High temperature nanoscratching of single crystal silicon under reduced oxygen condition. Materials Science and Engineering: A. **684**, 385-393 (2017).

21. S.Z. Chavoshi, S. Goel, and X. Luo: Molecular dynamics simulation investigation on the plastic flow behaviour of silicon during nanometric cutting. Modelling and Simulation in Materials Science and Engineering. **24**, 015002 (2015).
22. S.Z. Chavoshi and X. Luo: An atomistic simulation investigation on chip related phenomena in nanometric cutting of single crystal silicon at elevated temperatures. Computational Materials Science. **113**, 1-10 (2016).
23. S.Z. Chavoshi, S. Xu, and X. Luo: Dislocation-mediated plasticity in silicon during nanometric cutting: A molecular dynamics simulation study. Materials Science in Semiconductor Processing. **51**, 60-70 (2016).
24. S. Plimpton: Fast parallel algorithms for short-range molecular dynamics. Journal of computational physics. **117**, 1-19 (1995).
25. S. Xu, Y. Su, and S.Z. Chavoshi: Deformation of periodic nanovoid structures in Mg single crystals. Materials Research Express. (2018).
26. S.Z. Chavoshi, S. Goel, and X. Luo: Influence of temperature on the anisotropic cutting behaviour of single crystal silicon: A molecular dynamics simulation investigation. Journal of Manufacturing Processes. **23**, 201-210 (2016).
27. S.Z. Chavoshi, S. Xu, and S. Goel: Addressing the discrepancy of finding the equilibrium melting point of silicon using molecular dynamics simulations. Proc. R. Soc. A. **473**, 20170084 (2017).
28. S.Z. Chavoshi and S. Xu: Nanoindentation/scratching at finite temperatures: Insights from atomistic-based modeling. Progress in Materials Science. **In Press**, (2018).
29. S. Xu and Y. Su: Dislocation nucleation from symmetric tilt grain boundaries in body-centered cubic vanadium. Physics Letters A. **382**, 1185-1189 (2018).
30. S. Xu, L. Xiong, Y. Chen, and D.L. McDowell: Comparing EAM potentials to model slip transfer of sequential mixed character dislocations across two symmetric tilt grain boundaries in Ni. JOM. **69**, 814-821 (2017).
31. P. Vashishta, R.K. Kalia, A. Nakano, and J.P. Rino: Interaction potential for silicon carbide: a molecular dynamics study of elastic constants and vibrational density of states for crystalline and amorphous silicon carbide. Journal of applied physics. **101**, 103515-103528 (2007).
32. G. Voronoi: New applications of continuous parameters in the theory of quadratic forms. Z. Reine Angew. Math. **134**, 198 (1908).
33. E. Maras, O. Trushin, A. Stukowski, T. Ala-Nissila, and H. Jonsson: Global transition path search for dislocation formation in Ge on Si (001). Computer Physics Communications. **205**, 13-21 (2016).
34. W. Tao, P. Cao, and H.S. Park: Atomistic simulation of the rate-dependent ductile-to-brittle failure transition in bicrystalline metal nanowires. Nano letters. **18**, 1296-1304 (2018).
35. H. Xie, F. Yin, T. Yu, G. Lu, and Y. Zhang: A new strain-rate-induced deformation mechanism of Cu nanowire: transition from dislocation nucleation to phase transformation. Acta Materialia. **85**, 191-198 (2015).
36. N. Gunkelmann, D.R. Tramontina, E.M. Bringa, and H.M. Urbassek: Morphological changes in polycrystalline Fe after compression and release. Journal of Applied Physics. **117**, 085901 (2015).
37. V. Turlo and T.J. Rupert: Grain boundary complexions and the strength of nanocrystalline metals: Dislocation emission and propagation. Acta Materialia. **151**, 100-111 (2018).
38. T.J. Rupert and C.A. Schuh: Mechanically driven grain boundary relaxation: a mechanism for cyclic hardening in nanocrystalline Ni. Philosophical Magazine Letters. **92**, 20-28 (2012).
39. A. Stukowski: Visualization and analysis of atomistic simulation data with OVITO–the Open Visualization Tool. Modelling and Simulation in Materials Science and Engineering. **18**, 015012 (2009).
40. G.J. Tucker, S. Tiwari, J.A. Zimmerman, and D.L. McDowell: Investigating the deformation of nanocrystalline copper with microscale kinematic metrics and molecular dynamics. Journal of the Mechanics and Physics of Solids. **60**, 471-486 (2012).

41. I. Szlufarska, A. Nakano, and P. Vashishta: A crossover in the mechanical response of nanocrystalline ceramics. Science. **309**, 911-914 (2005).
42. A. Stukowski and K. Albe: Extracting dislocations and non-dislocation crystal defects from atomistic simulation data. Modelling and Simulation in Materials Science and Engineering. **18**, 085001 (2010).
43. H.-P. Chen, R.K. Kalia, A. Nakano, P. Vashishta, and I. Szlufarska: Multimillion-atom nanoindentation simulation of crystalline silicon carbide: Orientation dependence and anisotropic pileup. Journal of Applied Physics. **102**, 063514 (2007).
44. A. Stukowski: Computational analysis methods in atomistic modeling of crystals. Jom. **66**, 399-407 (2014).
45. H. Zhou, S. Qu, and W. Yang: Toughening by nano-scaled twin boundaries in nanocrystals. Modelling and Simulation in Materials Science and Engineering. **18**, 065002 (2010).
46. F. Sansoz and J. Molinari: Mechanical behavior of Σ tilt grain boundaries in nanoscale Cu and Al: A quasicontinuum study. Acta Materialia. **53**, 1931-1944 (2005).
47. C. Zener: The micro-mechanism of fracture. Fracturing of metals. **3**, (1948).
48. A. Stroh: The formation of cracks as a result of plastic flow. Proc. R. Soc. Lond. A. **223**, 404-414 (1954).
49. K. Zhou, B. Liu, S. Shao, and Y. Yao: Molecular dynamics simulations of tension–compression asymmetry in nanocrystalline copper. Physics Letters A. **381**, 1163-1168 (2017).
50. A. Dongare, A. Rajendran, B. LaMattina, D. Brenner, and M. Zikry: Atomic-scale study of plastic-yield criterion in nanocrystalline Cu at high strain rates. Metallurgical and Materials Transactions A. **41**, 523 (2010).
51. J. Monk and D. Farkas: Tension–compression asymmetry and size effects in nanocrystalline Ni nanowires. Philosophical Magazine. **87**, 2233-2244 (2007).
52. T. Tsuru: Origin of tension-compression asymmetry in ultrafine-grained fcc metals. Physical Review Materials. **1**, 033604 (2017).